J Mol Model (2011) 17:2659–2668
DOI 10.1007/s00894-010-0945-8

ORIGINAL PAPER

Density functional theory study of the potassium complexation of an unsymmetrical 1,3-alternate calix[4]-crown-5-*N*-azacrown-5 bearing two different crown rings

Xiaoyan Zheng · Xueye Wang · Keqi Shen · Yuan Miao · Dan Ouyang

Received: 10 October 2010 / Accepted: 27 December 2010 / Published online: 26 January 2011

Abstract Theoretical studies of an unsymmetrical calix[4]-crown-5-*N*-azacrown-5 (**1**) in a fixed 1,3-alternate conformation and the complexes **1**·K^+(a), **1**·K^+(b), **1**·K^+(c) and **1**·K^+K^+ were performed using density functional theory (DFT) at the B3LYP/6-31G* level. The fully optimized geometric structures of the free macroligand and its 1:1 and 1:2 complexes, as obtained from DFT calculations, were used to perform natural bond orbital (NBO) analysis. The two main types of driving force metal–ligand and cation–π interactions were investigated. NBO analysis indicated that the stabilization interaction energies (E_2) for O…K^+ and N…K^+ are larger than the other intermolecular interactions in each complex. The significant increase in electron density in the RY* or LP* orbitals of K^+ results in strong host–guest interactions. In addition, the intermolecular interaction thermal energies (ΔE, ΔH, ΔG) were calculated by frequency analysis at the B3LYP/6-31G* level. For all structures, the most pronounced changes in the geometric parameters upon interaction are observed in the calix[4] arene molecule. The results indicate that both the intermolecular electrostatic interactions and the cation–π interactions between the metal ion and π orbitals of the two pairs that face the inverted benzene rings play a significant role.

X. Zheng · X. Wang (✉) · K. Shen · Y. Miao · D. Ouyang
Key Laboratory of Environmentally Friendly Chemistry,
College of Chemistry, Xiangtan University,
Xiangtan, Hunan 411105, People's Republic of China
e-mail: wxueye@xtu.edu.cn

X. Zheng · X. Wang · K. Shen · Y. Miao · D. Ouyang
Applications of Ministry of Education, College of Chemistry,
Xiangtan University,
Xiangtan, Hunan 411105, People's Republic of China

Keywords Calix[4]-crown-5-*N*-azacrown-5 · Density functional theory (DFT) · Natural bond orbital (NBO) · Supramolecular chemistry · Cation–π interactions

Introduction

Calix[4]arenes, which are macrocyclic compounds that are available in a variety of ring sizes, are of particular interest as inclusion hosts for ions and specific molecules [1]. They can exist in four different conformations: a cone, a partial cone, 1,2-alternate, and 1,3-alternate [2]. They are macrocyclic compounds that are not only readily available on a large scale, but also offer near-boundless possibilities for chemical modification. This makes them highly attractive as building blocks for more sophisticated and elaborate host molecules. A number of moieties have been attached to the calixarene framework in order to achieve specific molecular architectures (in terms of shape, size, and conformation) with particular properties. Calix[4]crowns are capable of forming complexes with alkali metal cations, so they represent one of the most extensively investigated class of synthetic macrobicyclic compounds [3]. Derivatives that are highly selective towards alkaline and alkaline-earth cations have been obtained by fitting a crown-ether component to the calixarene. Such calixcrown ethers in which appropriately sized crown rings are incorporated into the calixarene framework have also attracted intense interest as specific metal-selective extractants [4]. 1,3-Alternate calix-bis-crowns [5–10] have particularly interesting molecular features, including (i) HSAB-based (hard and soft acid and base) complexation, with "hard" oxygen atoms complementing the "hard" metal ion; (ii) size matching between the crown ether cavity and a

specific metal ion; (iii) two crown loops that are able to adopt a 1:2 complexation; and (iv) a π–cation interaction between the two rotated benzene rings in the 1,3-alternate conformation and the metal ion [11–13]. Although calix-bis-crowns have two cavities that can simultaneously capture two metal ions, they have been shown to have even worse extractability than calix-mono-crowns. This is probably due to not only electrostatic repulsion between the two metal ions but also an induced change in conformation that does not favor the binding of the second metal [14]. On the basis of previous studies, we recently investigated four topics regarding the complexation of calix-bis-crowns with K^+: (i) the selectivity of independent ionophoric binding sites of calix[4]-bis-crowns in 1:1 complexes towards K^+; (ii) cation–π interactions between the metal ion K^+ and the two pairs of benzene rings; (iii) the effects of cation–cation repulsion on the cation interaction. We selected the compound calix[4]-crown-5-*N*-azacrown-5 (**1**) as a 1,3-alternate calix[4]-bis-crown with two different crown ether loops, as shown in Fig. 1.

The rapid development of hardware and constant improvements in computer coding make high-performance computational techniques a promising alternative to experimental studies. This is especially attractive when the experimental data are not available or incomplete. Nowadays, theoretical methods are used for small molecular systems and large biomolecules and biopolymers. In the framework of the density functional theory (DFT) approach, the B3LYP hybrid functional [15, 16] is one of the most popular methods as it has been shown to be reliable for reproducing various molecular properties, including structural parameters and vibrational spectra. The combined use of the B3LYP functional and the standard split valence basis set 6-31G* has been previously shown to provide an excellent compromise between accuracy and computational efficiency for the properties of large and medium-sized molecules [17–23]. Recently, considerable progress has been made in the quantum modeling of supermolecules. Density functional studies of hydroxylated calix[4]arene [24, 25], thiacalix[4]arene [26], and tetramethoxycalix[4]arene [27] have been published. The 1,3-alternate-25,27-bis(1-octyloxy)calix[4]arene-crown-6-H_3O^+ complex species [28] and the equilibrium structure of the complex 25,27-dihydroxycalix[4]arene-crown-6 (fixed in the 1,3-alternate conformation) with a cesium cation have also been investigated by B3LYP/6-31G* or B3LYP/6-31G** methods [29]. Considering the sizes and the complex structures of the systems that we are studying, the DFT method at the B3LYP/6-31G* level was chosen for use in this work.

The objective of this study was to handle large species precisely and provide a better understanding of the molecular behavior of the representative complexation between an unsymmetrical calix[4]-crown-5-*N*-azacrown-5 (**1**), which has both a conventional crown-5 and an *N*-azacrown-5 ring in a fixed 1,3-alternate conformation, and the alkali cation K^+. The molecule chosen for study is shown in Fig. 1.

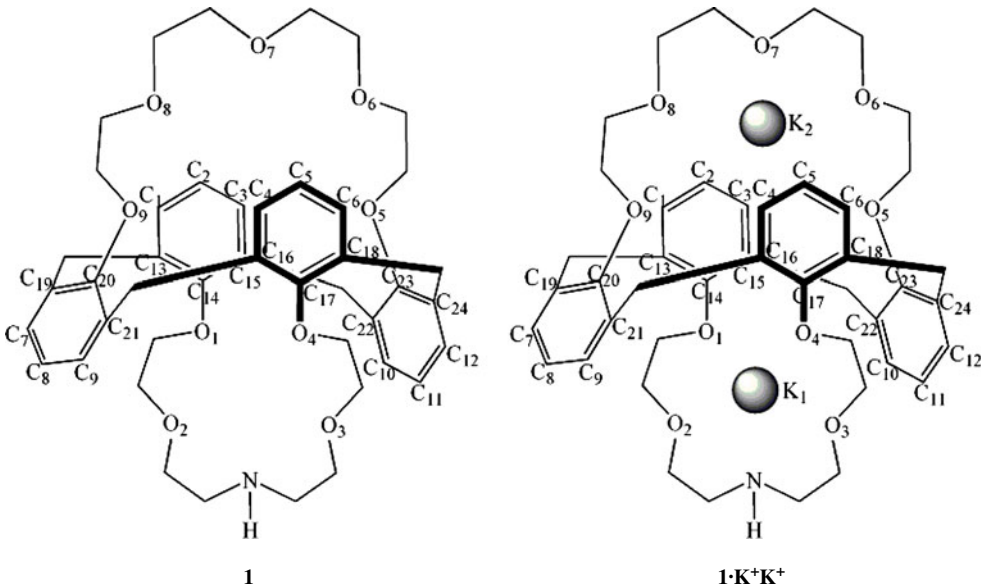

1 **1·K⁺K⁺**

1·K^+(a): a 1:1 complex, in which potassium coordinates with the N-azacrown-5 ring of the ligand **1**.
1·K^+(b): a 1:1 complex, in which potassium coordinates with the π-tube formed by the four benzene rings of the ligand **1**.
1·K^+(c): a 1:1 complex, in which potassium coordinates with the conventional crown-5 ring of the ligand **1**.
1·K^+ K^+: a 1:2 complex, in which two potassium ions coordinates with both the conventional crown-5 and the N-azacrown-5 rings of the ligand **1**.

Fig. 1 Chemical structures of the used species

Computational methods

The geometrical structures of the studied ligand **1** and its inclusion complexes $\mathbf{1}\cdot K^+$(a), $\mathbf{1}\cdot K^+$(b), $\mathbf{1}\cdot K^+$(c), and $\mathbf{1}\cdot K^+K^+$ with K^+ were fully optimized using density functional theory (DFT) methods, the 6-31G* basis set, the exchange potential of Becke [15], and the correlation functional of Lee, Yang and Parr [16] (B3LYP). Calculations were performed with the Gaussian 03W software package [30]. Harmonic vibrational frequencies and intensities were evaluated and natural bond orbital (NBO) analysis [31–34] was performed for both the free macroligand (**1**) and its complexes at the B3LYP/6-31G* level for all the stable structures.

The binding energies (ΔE), binding enthalpies (ΔH) and Gibbs free energies (ΔG) in the gas phase were calculated for the following reactions:

$$1_{\text{free}} + K^+_{\text{free}} \rightarrow 1\cdot K^+_{\text{complex}} \quad (1)$$

$$1_{\text{free}} + 2K^+_{\text{free}} \rightarrow 1\cdot K^+K^+_{\text{complex}}. \quad (2)$$

The binding energies ΔE for these reactions can be expressed as follows:

$$\Delta E = E(1\cdot K^+)_{\text{complex}} - E(1_{\text{free}}) - E\left(K^+_{\text{free}}\right) \quad (3)$$

$$\Delta E = E(1\cdot K^+K^+)_{\text{complex}} - E(1_{\text{free}}) - 2E\left(K^+_{\text{free}}\right). \quad (4)$$

The results of these calculations are reported below, and it is expected that they will be useful for experimental researchers in this field.

Results and discussion

The structures of the molecules play a crucial role in determining their chemical properties. Therefore, in order to study the most stable geometries of the unsymmetrical free ligand 1,3-alternate-calix[4]-crown-5-*N*-azacrown-5 (1) and its complexes $\mathbf{1}\cdot K^+$(a), $\mathbf{1}\cdot K^+$(b), $\mathbf{1}\cdot K^+$(c) and $\mathbf{1}\cdot K^+K^+$, the fully optimized geometries were derived. In the present section, these computational results are reported and their characteristic structures are discussed.

Optimized geometry

*Optimized geometry of the macroligand **1***

Calix[4]-crown-5-N-azacrown-5 (**1**) is a calix[4]arene moiety with four phenyl rings arranged alternately in an anti orientation and two different polyether fragments attached to the two rims of calix[4]arene. The 1,3-alternate-calix[4]arene has some interesting and unique structural characteristics that the other three conformers do not possess: (i) a metal-binding site composed of two "hard" oxygenic oxygens and two "soft" π-basic benzene rings; (ii) two independent ionophoric binding sites at both edges of the calix[4]arene cavity [35]; and (iii) two binding sites linked to each other by a π-basic tunnel surrounded by four benzene rings [36–39]. This suggests that there is a big cavity inside the molecule that may have the potential to form host–guest complexes. In order to better understand the structural properties of the macroligand **1**, its optimized structure (as calculated in this work and shown in Fig. 2) is discussed here. The optimizations performed in this work yield true minima, as the frequency calculations have no zero or negative eigenvalues.

The optimized structure of macroligand **1** is presented in Fig. 2. It shows that the calix[4]arene is fixed in a 1,3-alternate conformation by two macrocyclic polyether chains whose donor heteroatoms are separated by $-(CH_2)_2-$ groups. The central oxygen atom in one of the conventional crown-5 rings has been replaced by a –NH– group, so the free ligand is unsymmetrical. The bond angles associated with the bridging methylenes, i.e., C13-C25-C19, C15-C26-C22, C18-C27-C24 and C16-C28-C21, are 120.8(5)°, 120.6(5)°, 117.8(3)° and 118.0(9)°, respectively. All of these are all greater than the normal tetrahedral angle, due to repulsions among the four phenyl groups. The dihedral angles between the mean plane defined by the four methylenic carbon atoms (rms deviation 2.472) and the four aromatic rings are 52.4(4)°, 46.7(6)°, 52.5(1)° and 53.7

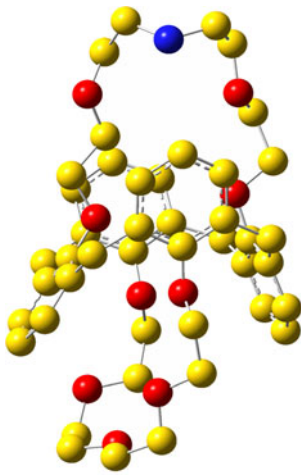

1

Fig. 2 The optimized structure of macroligand **1**, calculated at the B3LYP/6-31G* level. The *red spheres*, *blue spheres* and *yellow spheres* refer to O, N and C atoms, respectively. Hydrogen atoms are omitted for clarity

(2)°, respectively, which indicate that this structure is far less regular than is usual among this family of compounds. Four benzene rings are not perpendicular to the mean plane, as previously described [40]. Also, if we consider the two different substitutions of the calix[4]arene, the upper crown-5 fragment and the the lower *N*-azacrown-5 fragment cannot overlap perfectly with each other. There are some inward rotations which bring the unshared electron pairs of four phenolic oxygens into the cavity. Thus, the para carbons move away from each other in the facing benzene rings, as in the rim of a cup.

Optimized geometries of the 1:1 complexes

In **1**·K^+(a), the interatomic distances between K^+ and the electron-donating heteroatoms (N and O1–O4) are 3.175, 2.694, 4.355, 2.886 and 2.585 Å, respectively. The backbone structure of the polyether fragment adopts an ellipsoidal conformation and K^+ is not encapsulated in the middle of the *N*-azacrown-5 loop; it is located on one side of the *N*-azacrown-5 fragment, which is near to the donor atoms O1, O3 and O4 and far from N and O2. However, in **1**·K^+(c), the distances from K^+ to O5–O9 are 2.831, 2.877, 2.924, 2.876 and 2.820 Å, respectively. It is clear that the interatomic distances between K^+ and the five heteroatoms O5–O9 that participate in coordination are almost equal (the average distance is about 2.867 Å). In other words, K^+ is located at the center of the conventional crown-5 ring. The optimized geometries of the 1:1 complexes are shown in Fig. 3.

From Table 1, the distances from K^+ to C(7–12) in **1**·K^+(a) and from K^+ to C(1–6) in **1**·K^+(c) are 3.495, 3.506, 3.413, 3.474, 3.423, 3.374 Å and 3.408, 3.366, 3.396, 3.418, 3.304, 3.349 Å, respectively. It is obvious that all of the distances above are short, and that the distances in **1**·K^+(c) are shorter than those in **1**·K^+(a). Why are the interatomic K–C distances all quite similar after coordination in the inverted phenyl units? The oxygen atoms in these phenyl units do not interact with K^+ because they are too far apart. The results can be explained by the interactions of K^+ with the benzene rings: K^+ is trapped in a cavity consisting of phenolic oxygens, polyether oxygens and two π-basic benzene rings by both metal–oxygen electrostatic interactions and cation–π interactions. Considering the cation–π interactions between K^+ and the meta and para carbons of the two rotated benzene rings, the sum of the half-thickness of benzene's *p* orbital (1.70 Å) and the radius of K^+ (1.33 Å) is 3.03 Å [41]. Thus, the distances are close enough for cation–π interactions. Also, the cation–π interactions in **1**·K^+(a) are slightly stronger than those in **1**·K^+(c). This can be ascribed to the different locations of K^+. In **1**·K^+(a), K^+ is closer to the π tube formed by the four benzene rings. It should be noted that in **1**·K^+(a), the *N*-azacrown-5 fragment bound to calix[4]arene is still perpendicular to the mean plane after coordination. The presence of K^+ in the cavity of calix[4]-bis-crown-5 does not result in molecular reorganization. However, in contrast to O–K^+ electrostatic interactions, the cation–π interactions between K^+ and the π orbitals of the two pairs of rotated benzene rings are much weaker. It can thus be concluded that K^+ favors the conventional crown-5 part rather than the *N*-azacrown-5 loop with a 1:1 ligand–metal ion ratio. Thus, **1**·K^+(c) is much more stable than **1**·K^+(a), which can be attributed to the higher ability of K^+ to bind to the conventional crown-5 than the *N*-azacrown loop.

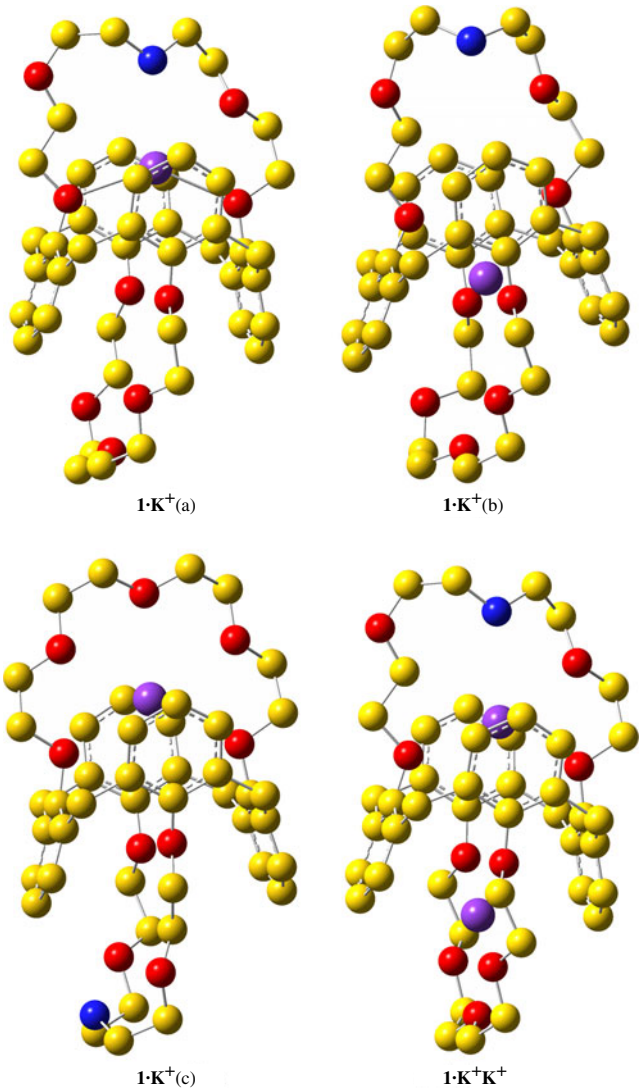

Fig. 3 Optimized structures of the complexes **1**·K^+(a), **1**·K^+(b), **1**·K^+(c), and **1**·K^+K^+, calculated at the B3LYP/6-31G* level. The *red spheres*, *blue spheres* and *yellow spheres* refer to O, N and C atoms, respectively. The *violet spheres* represent K^+. Hydrogen atoms are omitted for the sake of clarity

Table 1 Selected interatomic distances between K^+ and oxygen atoms of the polyether fragment and some of the carbon atoms in the π tube formed by the four phenyl units in the 1:1 and 1:2 complexes $\mathbf{1}\cdot K^+$(a), $\mathbf{1}\cdot K^+$(b), $\mathbf{1}\cdot K^+$(c), $\mathbf{1}\cdot K^+K^+$, optimized at the B3LYP/6-31G* level (distances in Å)

Bond	$\mathbf{1}\cdot K^+$(a)	Bond	$\mathbf{1}\cdot K^+$(a)	Bond	$\mathbf{1}\cdot K^+$(a)
K–N	3.175	K–O1	2.694	K–O2	4.355
K–O3	2.886	K–O4	2.585	K–O5	4.049
K–O9	4.403	K–C7	3.495	K–C8	3.506
K–C9	3.413	K–C10	3.474	K–C11	3.423
K–C12	3.374				
Bond	$\mathbf{1}\cdot K^+$(b)	Bond	$\mathbf{1}\cdot K^+$(b)	Bond	$\mathbf{1}\cdot K^+$(b)
K–N	6.971	K–O1	2.744	K–O2	5.946
K–O3	5.515	K–O4	3.127	K–O5	2.590
K–O6	4.755	K–O7	4.788	K–O8	3.990
K–O9	2.556	K–C13	3.189	K–C14	2.755
K–C15	3.122	K–C16	3.092	K–C17	2.836
K–C18	3.125	K–C19	3.462	K–C20	2.902
K–C21	3.448	K–C22	3.400	K–C23	2.869
K–C24	3.426				
bond	$\mathbf{1}\cdot K^+$(c)	Bond	$\mathbf{1}\cdot K^+$(c)	Bond	$\mathbf{1}\cdot K^+$(c)
K–O1	4.361	K–O4	4.814	K–O5	2.831
K–O6	2.877	K–O7	2.924	K–O8	2.876
K–O9	2.820	K–C1	3.408	K–C2	3.366
K–C3	3.396	K–C4	3.418	K–C5	3.304
K–C6	3.349				
Bond	$\mathbf{1}\cdot K^+K^+$	Bond	$\mathbf{1}\cdot K^+K^+$	Bond	$\mathbf{1}\cdot K^+K^+$
K1–N	3.214	K1–O1	2.738	K1–O2	4.345
K1–O3	2.715	K1–O4	2.587	K1–O5	4.554
K1–O9	4.572	K1–C7	3.445	K1–C8	3.365
K1–C9	3.336	K1–C10	3.506	K1–C11	3.433
K1–C12	3.392	K2–O5	2.877	K2–O6	2.785
K2– O7	2.793	K2–O8	2.786	K2–O9	2.880
K2–O1	4.868	K2–O4	5.013	K2–C1	3.489
K2–C2	3.377	K2–C3	3.499	K2–C4	3.523
K2–C5	3.412	K2–C6	3.549		

Optimized geometry of the transition state

It is well known that calix[4]arenes can be useful 3-D molecular building blocks for the synthesis of receptors with specific properties. The two ligating sites (crown-5 and azacrown-5) on the calix[4]arene framework are connected by a "hole" surrounded by four benzene rings. The π-tube hole can bind a metal ion. To illustrate all cases of coordination between macroligand **1** and K^+, we will focus on $\mathbf{1}\cdot K^+$(b) here. The optimized structure and key structural parameters are shown in Fig. 2 and Table 2, respectively. It should be noted that there is an imaginary frequency (-37.02 cm^{-1}) associated with this structure, because $\mathbf{1}\cdot K^+$(b) is a transition state between $\mathbf{1}\cdot K^+$(a) and $\mathbf{1}\cdot K^+$(c). Upon inspecting $\mathbf{1}\cdot K^+$(b), the distances for K^+–O1, K^+–O4, K^+–O5 and K^+–O9 are 2.744, 3.127, 2.590 and 2.556 Å, respectively. It is obvious that K^+ can coordinate to all four phenolic oxygens, and the former two K^+–O distances are longer than the latter two. K^+ does not position itself right in the middle of the π-tube cavity, but instead places itself closer to the conventional crown-5 ring than the azacrown-5 fragment. The distances from K^+ to C (13–18) in the *N*-azacrown-5 fragment and from K^+ to C (19–24) in the conventional crown-5 fragment are 3.189, 2.755, 3.122, 3.092, 2.836, 3.125 Å, and 3.462, 2.902, 3.448, 3.400, 2.869, 3.426 Å, respectively. The distances are close enough for cation–π interactions between K^+ and the ortho carbons of the two pairs of rotated benzene rings. In addition, the bond angle of C14-K-C17 was observed to be greater than that of C20-K-C23, implying that the K^+ surrounded by four benzene rings is closer to the conventional crown-5 side due to the drop in stability caused by the replacement of the central O atom with the –NH group.

Optimized geometry of the 1:2 complex

Observing the optimized structure of the 1:2 complex $\mathbf{1}\cdot K^+K^+$, interesting points regarding the distances between the two potassium ions (K1 and K2) and electron-donating heteroatoms (N and O) in crown-ether loops of the calix[4]arene can be noted. As listed in Table 1, the distances from K1 to N and O1–O4 in the upper *N*-azacrown-5 fragment are 3.214, 2.738, 4.345, 2.715 and 2.587 Å, respectively. For the lower crown-5 fragment, the distances from K2 to O5–O9 are 2.877, 2.785, 2.793, 2.786 and 2.880 Å, respectively. It is obvious that the distances from K1 to N and O_2 are much greater than those from K1 to the other three oxygen atoms. K1 does not fit into the *N*-azacrown-5 ring well. However, K2 positions itself at the center of the crown-5 ring. On the basis of a general "size concept" [42–44], the conventional crown-5 loop is more compatible with the K^+ ion than *N*-azacrown-5 is. Inspecting the optimized structure of $1\cdot K^+K^+$, the distances from K1 to C (7–12) (3.445, 3.365, 3.336, 3.506, 3.433, 3.392 Å) are slightly shorter than those from K2 to C(1–6) (3.489, 3.377, 3.499, 3.523, 3.412 and 3.549 Å). The distances are small enough for K^+–π interactions between K^+ and the meta and para carbons of the rotated benzene rings. The bond angle of C8-K1-C11 (170.593°) was found to be greater than that of C2-K2-C5 (172.881°), implying that K1 is closer to the π-basic tube formed by the four phenyl rings. It indicates that the cation–π interactions in the upper *N*-azacrown-5 ring are slightly greater than those in the conventional crown-5 loop. Therefore, in the 1:2 complex, K^+ seems to be more tightly encapsulated by the conventional crown-5 than by *N*-azacrown-5. The optimized geometries of the 1:2 complex are shown in Fig. 3.

Table 2 Selected stabilization interaction energies E_2 (kcal mol^{-1}) for **1**·K$^+$(a)

Donor NBO (i)→acceptor NBO(j)	E_2	Donor NBO (i)→acceptor NBO(j)	E_2	Donor NBO (i)→acceptor NBO(j)	E_2
CR N→LP*K	0.48	LP1 O1→RY*K	0.06	LP2 O4→RY*K	0.16
CR O2→LP*K	0.07	LP1 O1→RY*K	0.07	LP2 O4→RY*K	0.07
CR O1→LP*K	0.92	LP1 O1→RY*K	0.08	LP1 O3→LP*K	4.13
CR O4→LP*K	0.98	LP2 O1→LP*K	3.30	LP1 O3→RY*K	0.07
CR O3→LP*K	0.74	LP2 O1→RY*K	0.08	LP1 O3→RY*K	0.10
CR O5→LP*K	0.11	LP2 O1→RY*K	0.06	LP2 O3→LP*K	0.26
CR O9→LP*K	0.06	LP2 O1→RY*K	0.14	LP2 O3→RY*K	0.06
LP1 N→LP*K	2.28	LP2 O1→RY*K	0.05	LP2 O3→RY*K	0.12
LP1 N→RY*K	0.07	LP1 O4→LP*K	3.72	LP2 O3→RY*K	0.12
LP1 N→RY*K	0.22	LP1 O4→RY*K	0.05	LP2 O3→RY*K	0.08
LP1 N→RY*K	0.06	LP1 O4→RY*K	0.17	LP1 O5→LP*K	0.60
LP1 O2→LP*K	0.30	LP1 O4→RY*K	0.13	LP2 O5→LP*K	0.57
LP1 O1→LP*K	1.90	LP2 O4→LP*K	1.42	LP1 O9→LP*K	0.34
LP2 O9→LP*K	0.18				

CR 1-center core pair, *LP* 1-center valence lone pair (LP1 and LP2 are the two lone pairs of each oxygen atom, respectively; one of the NBOs is in the plane, and the other is the corresponding NBO perpendicular to the plane), *RY** 1-center Rydberg, *LP** 1-center valence antibond lone pair

From this point of view, it is possible that combining polyether fragments and calix[4]arene would result in an optimized structure for metal ion encapsulation, due to (1) electrostatic interactions between K^+ and the heteroatoms (O and N), and (2) cation–π interactions between K^+ and the two rotated aromatic nuclei of 1,3-alternate calix[4] arene. Although the cation–π interaction between K^+ and a single carbon atom is very small, the presence of multiple cation–π interactions can greatly enhance host–guest interactions. Thus, both electrostatic and cation–π interactions are the main driving forces for the coordination between calix[4]-bis-crown-5 and K^+.

NBO analysis

It is useful to review some interesting concepts relating to NBO analysis, which is used very effectively in this work. In NBO analysis, the electronic wavefunctions are interpreted in terms of a set of occupied Lewis and unoccupied non-Lewis localized orbitals. Delocalization of electron density between occupied Lewis-type (bond or lone-pair) NBO orbitals and formally unoccupied non-Lewis-type (antibond) NBO orbitals corresponds to a stabilizing donor–acceptor interaction, which is taken into consideration by examining all possible interactions between filled (donor) and empty (acceptor) orbitals, and then evaluating their energies by second-order perturbation theory. Accordingly, the delocalization effects (or donor–acceptor charge transfers) can be estimated from the presence of off-diagonal elements of the Fock matrix in the NBO basis. NBOs closely correspond to the picture of localized bonds and lone pairs as basic units of molecular structure, so that is possible to interpret wavefunctions conveniently ab initio in terms of the classical Lewis structure concepts by transforming these functions into NBO form. The interactions due to electron delocalization are generally analyzed by selecting a number of bonding and antibonding NBOs (those relevant to the analysis of donor and acceptor properties). As a result, the NBO program searches for an optimal natural Lewis structure that exhibits the maximum occupancy of its occupied NBOs and in general agrees with the pattern of bonds and lone pairs of the standard structural Lewis formula. However, these orbitals suffer from small departures from the idealized Lewis structure. These departures are caused by interactions among the orbitals, which are known as hyperconjugative or stereoelectronic interactions. Therefore, the new orbitals are more stable than pure Lewis orbitals, which stabilizes the wavefunction and leads to a set of molecular orbitals that are equivalent to canonical molecular orbitals. For each donor NBO (i) and acceptor NBO (j), the stabilization energy (E_2) associated with $i \rightarrow j$ delocalization is explicitly estimated by the following equation:

$$E_2 = \Delta E_{ij} = q_i \frac{F^2(i,j)}{\varepsilon_j - \varepsilon_i}, \quad (5)$$

where q_i is the ith donor orbital occupancy, ε_i and ε_j are diagonal elements (orbital energies), and $F(i,j)$ are off-diagonal elements, respectively, associated with the NBO Fock matrix.

The second-order perturbation stabilization energies E_2 obtained by NBO analysis are summarized in Tables 2, 3, 4, 5. These can be used to describe the interactions between the macroligand and K^+. In NBO analysis, if the stabilization interaction energy E_2 between a donor bonding orbital and an acceptor antibonding orbital is large, there is a strong interaction between the two orbitals. As shown in Tables 2 to 5, the interaction energies E_2 of the host–guest

Table 3 Selected stabilization interaction energies E_2 (kcal mol^{-1}) for **1**·K$^+$(b)

Donor NBO (i)→acceptor NBO(j)	E_2	Donor NBO (i)→acceptor NBO(j)	E_2	Donor NBO (i)→acceptor NBO(j)	E_2
CR O6→LP*K	0.13	LP2 O1→LP*K	1.42	LP2 O6→LP*K	0.10
CR O7→LP*K	0.12	LP2 O1→RY*K	0.05	LP1 O7→LP*K	0.94
CR O5→LP*K	0.30	LP1 O4→LP*K	0.31	LP2 O7→LP*K	0.13
CR O8→LP*K	0.22	LP2 O4→LP*K	1.79	LP1 O5→LP*K	1.49
CR O9→LP*K	0.29	LP2 O4→RY*K	0.09	LP2 O5→LP*K	0.95
LP1 O2→LP*K	0.21	LP1 O3→LP*K	0.41	LP1 O8→LP*K	1.66
LP1 O1→LP*K	0.96	LP1 O6→LP*K	0.81	LP2 O8→LP*K	0.11
LP1 O9→LP*K	1.32	LP2 O9→LP*K	0.98		

molecules are mainly caused by the lone-pair electrons of the heteroatoms N or O and the RY* or LP* orbitals of K$^+$.

As shown in Table 2, in **1**·K$^+$(a) there are strong donor–acceptor interactions between the LP(1) N, LP(1) O1, LP(1) O3, LP(1) O4, and LP(2) O4 orbitals of macroligand **1** and the RY* or LP* orbitals of K$^+$, which have E_2 values of 2.28, 1.90, 3.30, 4.13, 3.72, 1.42 kcal mol^{-1}, respectively. In **1**·K$^+$(c), there are strong donor–acceptor interactions between the LP(1) orbitals of O5–O9 of macroligand **1** and the RY* or LP* orbitals of K$^+$, and the corresponding E_2 values (in Table 4) are 1.91, 2.16, 2.26, 2.17 and 1.95 kcal mol^{-1}, respectively. Although both **1**·K$^+$(a) and **1**·K$^+$(c) have strong K$^+$–O electrostatic interactions, the situation is much different. In **1**·K$^+$(a), the main interactions are not caused by all of the donor atoms of the *N*-azacrown-5 fragment: the contributions of the participating donor atoms (N, O1, O3 and O4) are not equal. Thus, the cavity size of the *N*-azacrown-5 is not a perfect fit for K$^+$. In **1**·K$^+$(c), the five donor atoms (O5–O9) taking part in metal–ligand interactions provide almost equal contributions. Also, before and after coordination, the backbone of the optimized structure **1**·K$^+$(c) shows little distortion. On the basis of a general "size concept" [42], the conventional crown-5 is a better complement to K$^+$.

In **1**·K$^+$(b), K$^+$ positions itself in the π-basic tube of macroligand **1**, and the four phenolic oxygens in both the *N*-azacrown-5 and the conventional crown-5 rings take part in coordination. As shown in Table 3, there are strong donor–acceptor interactions between the LP(2) O1, LP(2) O4, LP(1) O5, and LP(1) O8 orbitals of macroligand **1** and the RY* or LP* orbitals of K$^+$, which have E_2 values of 1.42, 1.79, 1.49, 1.66 kcal mol^{-1}, respectively. It is clear that the E_2 values for **1**·K$^+$(b) are smaller than the corresponding values in the complexes **1**·K$^+$(a) and **1**·K$^+$(c).

In **1**·K$^+$K$^+$, the stabilization energies (E_2) are also influenced by the lone-pair electrons of the electron-donating O or N atoms and the RY* or LP* orbitals of K$^+$. Upon inspecting Table 5, the E_2 values for the upper N-azacrown-5 fragment of calix[4]arene, which are due to N (LP1), O1 (LP2), O3 (LP1), O4 (LP1), and O4 (LP2), are 1.57, 2.20, 1.54, 2.19, 1.06 kcal mol^{-1}, respectively. For the lower crown-5 fragment, the corresponding values caused by O5–O9 and K$^+$ are 2.54, 2.37, 2.46, 2.37 and 2.54 kcal mol^{-1}, respectively. It is clear that the stabilization energies (E_2) caused by the crown-5 fragment are greater than those due to the *N*-azacrown-5 fragment.

In NBO analysis, the importance of hyperconjugation interactions and electron density transfer (EDT) from the lone-pair electrons of atom Y to the M$^+$ antibonding orbital in the Y…M$^+$ system is well documented [35]. In general, such interactions lead to an increase in the population of the M$^+$ antibonding orbital. Based on theoretical analysis, we find that the stabilization interaction energy E_2 for Y…M$^+$ is relatively large. The remarkable increase in the electron densities of the RY* or LP* orbitals of M$^+$ results in strong interactions between macroligand **1** and K$^+$. These results

Table 4 Selected stabilization interaction energies E_2 (kcal mol^{-1}) for **1**·K$^+$(c)

Donor NBO (i)→acceptor NBO(j)	E_2	Donor NBO (i)→acceptor NBO(j)	E_2	Donor NBO (i)→acceptor NBO(j)	E_2
CR O6→LP*K	0.30	LP1 O4→LP*K	0.28	LP1 O5→LP*K	1.91
CR O7→LP*K	0.30	LP2 O4→LP*K	0.41	LP2 O5→LP*K	0.68
CR O5→LP*K	0.29	LP1 O6→LP*K	2.16	LP1 O8→LP*K	2.17
CR O8→LP*K	0.30	LP2 O6→RY*K	0.07	LP2 O8→RY*K	0.07
CR O9→LP*K	0.29	LP1 O7→LP*K	2.26	LP1 O9→LP*K	1.95
LP1 O1→LP*K	0.39	LP1 O7→RY*K	0.06	LP2 O9→LP*K	0.64
LP2 O1→LP*K	0.64	LP2 O7→RY*K	0.09		

Table 5 Selected stabilization interaction energies E_2 (kcal mol^{-1}) for **1**· K^+K^+

Donor NBO (i)→acceptor NBO(j)	E_2	Donor NBO (i)→acceptor NBO(j)	E_2	Donor NBO (i)→acceptor NBO(j)	E_2
CR N→LP*K1	0.30	LP1 N→LP*K1	1.57	LP1 O3→LP*K1	2.54
CR O2→LP*K1	0.13	LP1 N→RY*K1	0.08	LP2 O3→LP*K1	0.12
CR O1→LP*K1	0.45	LP1 O2→LP*K1	0.73	LP2 O3→RY*K1	0.06
CR O4→LP*K1	0.50	LP1 O1→LP*K1	0.21	LP1 O5→LP*K1	0.30
CR O3→LP*K1	0.50	LP2 O1→LP*K1	2.20	LP2 O5→LP*K1	0.18
CR O5→LP*K1	0.08	LP1 O4→LP*K1	2.19	LP1 O9→LP*K1	0.30
CR O9→LP*K1	0.08	LP2 O4→LP*K1	1.06	LP2 O9→LP*K1	0.18
CR O6→LP*K2	0.32	LP1 O4→LP*K2	0.16	LP2 O7→RY*K2	0.06
CR O7→LP*K2	0.32	LP2 O4→LP*K2	0.15	LP1 O5→LP*K2	1.54
CR O5→LP*K2	0.28	LP1 O6→LP*K2	2.37	LP2 O5→LP*K2	0.98
CR O8→LP*K2	0.32	LP2 O6→RY*K2	0.06	LP1 O8→LP*K2	2.37
CR O9→LP*K2	0.28	LP1 O7→LP*K2	2.46	LP2 O8→RY*K2	0.05
LP2 O1→LP*K2	0.31	LP1 O7→RY*K2	0.06	LP1 O9→LP*K2	2.54
LP 2 O9→LP*K2	0.99				

indicate that, during the course of coordination, electrostatic interactions between K^+ and heteroatoms (O and N) at both edges of macroligand **1** play an important role.

Binding energies and stabilities

The binding energies (ΔE), binding enthalpies (ΔH) and Gibbs free energies (ΔG) at 298 K of the complexes **1**·K^+(a), **1**·K^+(b), **1**·K^+(c), and **1**·K^+K^+ formed by calix[4]-crown-5-*N*-azacrown-5 (**1**) and K^+, based on reactions 3 and 4, and calculated using DFT methods at the B3LYP/6-31G* level, are listed in Table 6.

Table 6 indicates that the calculated binding energies (ΔE), enthalpies (ΔH) and Gibbs free energies (ΔG) (at 298K) of the 1:1 complexes **1**·K^+(a), **1**·K^+(b), and **1**·K^+(c) in the gas phase decrease in the order **1**·K^+(c), **1**·K^+(a), **1**·K^+(b); in other words, $\Delta E^b_{1\cdot K(c)} > \Delta E^b_{1\cdot K(a)} > \Delta E^b_{1\cdot K(b)}$. In contrast to **1**·$K^+$(a) and **1**·$K^+$(c), during the course of coordination, the formation of **1**·K^+(c) releases more heat, and this complex is more stable than **1**·K^+(a), due to the different polyethers of the calix[4]arene. Therefore, in the gas phase at 298K, the conventional crown-5 fragment of the calix[4]arene displays better binding behavior than the modified *N*-azacrown-5 fragment does towards K^+. If we consider the 1:2 complex **1**·K^+K^+, the calculated binding energy (ΔE), enthalpy (ΔH) and Gibbs free energy (ΔG) (298K) are much smaller than twice the energies of the 1:1 complexes. Thus, the 1:1 complexes are more stable than the 1:2 complex. These results indicate that the order of stability of the complexes is: 1·K^+(c)>1·K^+(a)>1·K^+K^+ > 1·K^+(b).

In the literature [45, 46], the order of the experimental K_a values for the 1:1 inclusion complexes **1**·K^+(a) and **1**·K^+(c) in aqueous solution has been described as: **1**·K^+(a)>**1**·K^+(c). It has been reported that calix[4]-crown-5-*N*-azacrown-5 shows high selectivity and sensitivity towards potassium ion, but that different ionophoric binding sites have different binding abilities [14, 45, 46]. It is clear that the calculated order of interaction energies for the interaction in the gas phase between K^+ and macroligand **1** is not consistent with the experimental results. These pronounced differences between the theoretical results and experimental data result from the fact that our calculations are performed for isolated molecules in the gas phase, but the experiments were performed in aqueous solution. The presence of the polar solvent methanol affects the structures of the macroligand and the complexes. This solvent effect is known to influence the complexation and selectivities. For instance, dibenzo-18-crown-6 prefers K^+ in polar protic solvents (water, methanol) [42, 43], but Na^+ in acetonitrile [44]. 15-Crown-5 selectively complexes Na^+ in acetonitrile [47] and in pyridine [48], but K^+ in methanol [49], Cs^+ in water [50], and Li^+ in propylene carbonate [51]. In conclusion, the solvent effect plays an important role in the stabilization of a particular isomer. The most favorable isomer in the vacuum need not be the most preferred isomer in the polar environment. Usually structures of low polarity are stabilized in the vacuum and nonpolar

Table 6 The binding energies ΔE (kcal mol^{-1}), binding enthalpies ΔH (kcal mol^{-1}), and Gibbs free energies ΔG (kcal mol^{-1}) in the gas phase for the complexes **1**·K^+(a), **1**·K^+(b), **1**·K^+(c), and **1**·K^+K^+ at 298K

Complex	ΔE	ΔH	ΔG
1·K^+(a)	−70.59	−71.18	−65.26
1·K^+(b)	−49.36	−49.96	−46.96
1·K^+(c)	−93.68	−94.28	−88.13
1·K^+K^+	−106.06	−107.25	−99.86

solvents, but increasing the environmental polarity allows the stabilization of polar structures.

Conclusions

The fully optimized structures for calix[4]-crown-5-*N*-azacrown-5 (**1**) and its complexes with K^+, i.e., $\mathbf{1}\cdot K^+$(a), $\mathbf{1}\cdot K^+$(b), $\mathbf{1}\cdot K^+$(c) and $\mathbf{1}\cdot K^+K^+$, have been obtained by DFT calculations using the B3LYP method at the 6-31G* level, and the calculated results are useful. The energetic and structural preferences of calix[4]-crown-5-*N*-azacrown-5 with and without K^+ are presented for the first time, and DFT has been used to study the effects of electrostatic and cation–π interactions. This study established that the cation is bound to ionophoric binding sites consisting of two oxygenic ligands and two benzene rings with the aid of both electrostatic interactions and cation–π interactions. The computed effect is of interest not only from the perspective of the selectivity of the calix[4]-crown-5-*N*-azacrown-5 towards potassium ion in the formation of 1:1 and 1:2 complexes, but also from the viewpoint of the variety of synthetic hosts and biochemical systems that are capable of multiple cation–π interactions.

Acknowledgments The author wish to acknowledge financial support from the Scientific Research Fund of the Hunan Provincial Education Department (No. 09A091) for this research work.

References

1. Van Loon JD, Verboom W, Reinhoudt DN (1992) Org Prep Proced Int 24:437–462
2. Gutsche CD, Bauer LJ (1985) J Am Chem Soc 107:6052–6059
3. Böhmer V (1995) Angew Chem 34:713–745
4. Casnati A, Pochini A, Ungaro R, Ugozzoli F, Arnaud-Neu F, Fanni S, Schwing MJ, Egberink RJM, de Jong F, Reinhoudt DN (1995) J Am Chem Soc 117:2767–2777
5. Thuéry P, Nierlich M, Lamare V, Dozol JF, Asfari Z, Vicens J (2000) J Incl Phenom Macrocycl Chem 36:375–408
6. Kim JS, Suh IH, Kim JK, Cho MH (1998) J Chem Soc Perkin Trans 1:2307–2312
7. Kim JS, Ohki A, Ueki R, Ishizuka T, Shimotashiro T, Maeda S (1999) Talanta 48:705–710
8. Kim JS, Ohki A, Cho MH, Kim JK, Ra DY, Cho NS, Bartsch RA, Lee KW, Oh WZ (1997) Bull Korean Chem Soc 18:1014–1017
9. Kim JS, Lee WK, Ra DY, Lee YI, Choi WK, Lee KW, Oh WZ (1998) Microchem J 59:464–471
10. Kim JS, Pang JH, Yu IY, Lee WK, Suh IH, Kim JK, Cho MH, Kim ET, Ra DY (1999) J Chem Soc Perkin Trans 2:837–846
11. Asfari Z, Abidi R, Arnaud-Neu F, Vicens J (1992) J Incl Phenom 13:163–169
12. Asfari Z, Weiss J, Pappalardo S, Vicens J (1993) Pure Appl Chem 65:585–590
13. Hill C, Dozol JF, Lamare V, Rouquette H, Eymard S, Tournois B, Vicens J, Asfari Z, Bressot C, Ungaro R, Casnati A (1994) J Incl Phenom 19:399–408
14. Bouquant J, Delville A, Grandjean J, Laszlo P (1982) J Am Chem Soc 104:686–691
15. Becke AD (1993) J Chem Phys 98:5648–5652
16. Lee C, Yang W, Parr RG (1998) Phys Rev B 37:785–789
17. Korth HG, de Heer MI, Mulder P (2002) J Phys Chem A 106:8779–8789
18. Johnson BG, Gill PMW, Pople JA (1993) J Chem Phys 98:5612–5626
19. Chowdhury PK (2003) J Phys Chem A 107:5692–5696
20. Chis V (2004) Chem Phys 300:1–11
21. Asensio A, Kobko N, Dannenberg JJ (2003) J Phys Chem A 107:6441–6443
22. Müller A, Losada M, Leutwyler S (2004) J Phys Chem A 108:157–165
23. Gonçalves NS, Cristiano R, Pizzolatti MG, da Silva Miranda F (2005) J Mol Struct THEOCHEM 733:53–61
24. Bernardino RJ, Cabral BJC (1999) J Phys Chem A 103:9080–9085
25. Bernardino RJ, Cabral BJC (2002) Supramol Chem 14:57–66
26. Bemardino RJ, Cabral BJC (2001) J Mol Struct THEOCHEM 549:253–260
27. Hay BP, Nicholas JB, Feller D (2000) J Am Chem Soc 122:10083–10089
28. Dybal J, MakrlÍk E, Vaňura P, Budka J (2008) Monatsh Chem 139:1175–1178
29. Ilchenko NN, Kuchma OV, Zub YL, Leszczynski J (2007) J Mol Struct THEOCHEM 815:83–86
30. Frisch MJ, Trucks GW, Schlegel HB, Scuseria GE, Robb MA, Cheeseman JR, Montgomery JA Jr, Vreven T, Kudin KN, Burant JC, Millam JM, Iyengar SS, Tomasi J, Barone V, Mennucci B, Cossi M, Scalmani G, Rega N, Petersson GA, Nakatsuji H, Hada M, Ehara M, Toyota K, Fukuda R, Hasegawa J, Ishida M, Nakajima T, Honda Y, Kitao O, Nakai H, Klene M, Li X, Knox JE, Hratchian HP, Cross JB, Bakken V, Adamo C, Jaramillo J, Gomperts R, Stratmann RE, Yazyev O, Austin AJ, Cammi R, Pomeli C, Ochterski JW, Ayala PY, Morokuma K, Voth GA, Salavador P, Dannenberg JJ, Zakrewski VG, Dapprich S, Daniels AD, Strain MC, Farkas O, Malick DK, Rabuck AD, Raghavachari K, Foresman JB, Ortiz JV, Cui Q, Baboul AG, Clifford S, Cioslowski J, Stefanov BB, Liu G, Liashenko A, Piskorz P, Komaromi I, Martin RL, Fox DJ, Keith T, Al-Laham MA, Peng CY, Nanayakkara A, Challacombe M, Gill PMW, Johnson B, Chen W, Wong MW, Gonzalez C, Pople JA (2003) Gaussian 2003 W, revision B.05. Gaussian Inc., Pittsburgh
31. Reed AE, Weinhold F (1983) J Chem Phys 78:4066–4073
32. Foster JP, Weinhold F (1980) J Am Chem Soc 102:7211–7218
33. Redd AE, Weinstock RB, Weinhold F (1985) J Chem Phys 83:735–746
34. Reed AE, Curtiss LA, Weinhold F (1988) Chem Rev 88:899–926
35. Iwamoto K, Shinkai S (1992) J Org Chem 57:7066–7073
36. Bott SG, Coleman AW, Atwood JL (1987) J Incl Phenom Macrocycl Chem 5:747–758
37. Fujimoto K, Nishiyama N, Tsuzuki H, Shinkai S (1992) J Chem Soc Perkin Trans 2:643–648
38. Kikuchi T, Iki H, Tsuzuki H, Shinkai S (1993) Supramol Chem 1:103–106
39. Grootenhuis PDJ, Kollman PA, Groenen LC, Reinhoudt DN, van Hummel GJ, Ugozzoli F, Andreetti GD (1990) J Am Chem Soc 112:4165–4176
40. Macias AT, Norton JE, Evanseck JD (2003) J Am Chem Soc 125:2351–2360
41. Shannon RD (1976) Acta Crystallogr A 32:751–767
42. Shchori E, Nae N, Jagur-Grodzinski J (1975) J Chem Soc Dalton Trans 2:2381–2386
43. Kolthoff IM, Chantooni MK (1980) Anal Chem 52:1039–1044
44. Hofmanova A, Koryta J, Brezine M, Mitall M (1978) Inorg Chim Acta 28:73–76

45. Kima S, Kima H, Noh KH, Lee SH, Kimb SK, Kimc JS (2003) Talanta 61:709–716
46. Kim JS, Thuéry P, Nierlich M, Rim JA, Yang SH, Lee JK, Cho KH, Lee JH, Vicens J (2001) Bull Korean Chem Soc 22:321–324
47. Hopkins HP Jr, Norman AB (1980) J Phys Chem 84:309–314
48. Smetana AJ, Popov AI (1980) J Solution Chem 9:183–196
49. Lamb JD, Izatt RM, Swain CS, Christensen JJ (1980) J Am Chem Soc 102:475–479
50. Izatt RM, Terry RE, Haymore BL, Hansen LD, Dalley NK, Avondet AG, Christensen JJ (1976) J Am Chem Soc 98:7620–7626
51. Takeda Y, Yano H, Ishibashi M, Isozumi H (1980) Bull Chem Soc Jpn 53:72–76